Magnetic Resonance in Medicine 46:510–514 (2001)

Comparison of Functional MRI Image Realignment Tools Using a Computer-Generated Phantom

Victoria L. Morgan,[1*] David R. Pickens,[1] Steven L. Hartmann,[2] and Ronald R. Price[1]

This study discusses the development of a computer-generated phantom to compare the effects of image realignment programs on functional MRI (fMRI) pixel activation. The phantom is a whole-head MRI volume with added random noise, activation, and motion. It allows simulation of realistic head motions with controlled areas of activation. Without motion, the phantom shows the effects of realignment on motion-free data sets. Prior to realignment, the phantom illustrates some activation corruption due to motion. Finally, three widely used realignment packages are examined. The results showed that the most accurate algorithms are able to increase specificity through accurate realignment while maintaining sensitivity through effective resampling techniques. In fact, accurate realignment alone is not a powerful indicator of the most effective algorithm in terms of true activation. Magn Reson Med 46:510–514, 2001. © 2001 Wiley-Liss, Inc.

Key words: functional MRI; image registration; brain; BOLD; computer phantom

Functional MRI (fMRI) is a noninvasive imaging technique which takes advantage of small magnetic field distortions in cerebral blood flow to localize areas of the brain utilized during specific tasks (1–3). When a brain region is engaged to control a task, the blood flow to that area is increased in response to increased metabolic demand. This increase in blood flow is more than required by increased cellular oxygen demand and thus results in a regional increase in the local ratio of oxyhemoglobin to deoxyhemoglobin. Through the use of a T_2^*-weighted pulse sequence, this ratio shift can be detected as an MR signal increase. This signal increase is usually less than 5% at a field strength of 1.5T. To distinguish the areas of activation from noise, the brain is imaged repeatedly in both a baseline (rest) state and an activation state during which the brain is attending to a specific task. The areas of the brain used exclusively during the task are determined statistically by comparing signal intensities between the images acquired in each state. Comparison between the resting and activation states assumes no motion has occurred between the two states. This may be accomplished if the subject remains completely still throughout the acquisition. However, in most cases it is not possible for subjects to be completely motionless (4). Motion can be especially troublesome in those studies involving patients or children. This problem has led to the development of various image realignment programs.

Image registration programs are now available that correct for 2D (5–7) and 3D motion (6–13). Some algorithms are considered to be intensity-based (6–9,11–13), while others are feature-based (14). Some are combinations of both techniques (10). Our hypothesis is that these methods will have different results when applied to different types of motion and levels of activation. When conducting an fMRI study, the decision as to which type of algorithm would be most appropriate could be very important to the results. Previous comparisons of these algorithms have been either qualitative in nature or quantitative in spatial measurements of alignment of images. The first objective of this study was to develop a software phantom that would contain realistic head motions and predetermined areas of activation to facilitate quantitative comparisons of activation localization and intensity post realignment. The second objective was to test the validity of the phantom by comparing three of the most widely used algorithms using this technique. More than one version of each program has been included to illustrate changes and improvements in the algorithms.

METHODS

To compare the realignment methodologies, a phantom was created using IDL (Research Systems, Inc., Boulder, CO). A full brain volume collected from an adult male volunteer with an echo planar imaging (EPI) pulse sequence was used as the basis for the phantom (64 × 64, TE = 60 ms, TR = 4000 ms, 5 mm thick, 1 mm gap, 21 or 23 axial slices, FOV = 24 cm, 1.5 T GE Signa Horizon scanner). The volume was copied to create 76 identical temporal samples. Additional uniformly distributed random noise of no more than 5% of the pixel intensity was added to each pixel in each volume. Six different areas of activation were then added to the data set by increasing the intensity of the pixel by a designated percent during predetermined stimulus periods of 10 volumes interleaved with rest periods of 10 volumes (except for the first rest period, which is made up of six volumes). The percent increases were chosen as 1%, 1.5%, 2%, 2.5%, 3%, and 4% to approximate the level of activation commonly observed at 1.5T. For each signal increase, the area of activation covered three slices and was 36–90 pixels in size. No areas of activation were created on the edge of the brain. This phantom (without motion) was saved as the activation-only phantom.

Two "motion" phantoms were then created using the activation-only phantom. Phantom motion was derived using the center of mass motion of a blind volunteer reading Braille during an fMRI study. The coordinates of the center of mass were measured along three axes using Stimulate (15) and added to the phantom. Rotation about the x

[1]Department of Radiological Sciences, Vanderbilt University, Nashville, Tennessee.

[2]Department of Biomedical Engineering, Vanderbilt University, Nashville, Tennessee.

*Correspondence to: Victoria L. Morgan, Ph.D., Department of Radiological Sciences, R1318A Medical Center North, Vanderbilt University, Nashville, TN 37232-2675. E-mail: victoria.morgan@vanderbilt.edu

Received 5 June 2000; revised 26 March 2001; accepted 30 March 2001.

and *z* axes of less than 0.5° was added to each volume arbitrarily to reflect small up–down and right–left head tilts. The resulting image volumes were then saved as the rigid-body phantom. The second phantom used nonrigid-body motion maps derived from a normal volunteer performing a finger-tapping fMRI task using an in-house elastic registration program (16). This motion was then added to the activation-only phantom to create an elastic-motion phantom.

Three freely available realignment software packages were used to register the phantom data sets. All volumes were realigned with the first volume in the set. The details of each trial are given below:

1. SPM99b (8): SPM99b (release 5/17/99) with reslicing using sinc interpolation.
2. AFNI98 (13): AFNI 2.23.1 3D image registration plug-in using quintic resampling.
3. SPM96-0 (8): SPM 96 using sinc interpolation with no adjustment.
4. SPM96-2 (8): SPM96 using sinc interpolation with second-order adjustment.
5. AFNI96 (5): AFNI 2.01a 2D image registration plug-in run with no fine fitting.
6. AIR-L (6,7): AIR 3.08 linear 3D, rigid-body image alignment using the following parameters: 8 mm × 8mm × 8mm FWHM Gaussian spatial smoothing, scaled least-squares difference image cost function, secondary termination criteria = 25 total iterations or five iterations without improvement, sampling from every 81 to 1 voxel, a convergence threshold of 1.0, and image reslicing with trilinear interpolation.
7. AIR-W (6,7): AIR 3.08 nonlinear, 3D image alignment using the following parameters: third-order nonlinear 60-parameter model, 8 mm × 8 mm × 8 mm FWHM Gaussian spatial smoothing, secondary termination criteria = 50 total iterations or five iterations without improvement, sampling every 81 to 9 voxels, a convergence threshold of 0.1, and image reslicing with trilinear interpolation.

The results were compared based on three parameters: 1) percent of true-positive activations (sensitivity), 2) level of activation (percent signal change) of true-positive activations, and 3) number of false-positive activations (specificity). For each phantom, for each realignment method, a realigned data set was produced. Activation maps of each were determined using a *t*-test with $P < 0.05$ using Stimulate (15). In each area of activation, the percent of true-positive activations was defined as the number of pixels activated in the data set divided by the number of pixels in the region of interest (ROI) multiplied by 100%. The percent of expected signal change of each area of activation was defined as the percent signal change of the activated pixels in the data set divided by the percent signal change designed into the phantom in that ROI multiplied by 100%. In addition, the number of false-positive activations in the volume was counted.

RESULTS

An axial slice through the motion-free phantom is given in Fig. 1a. This image shows simulated activation (arrow) and

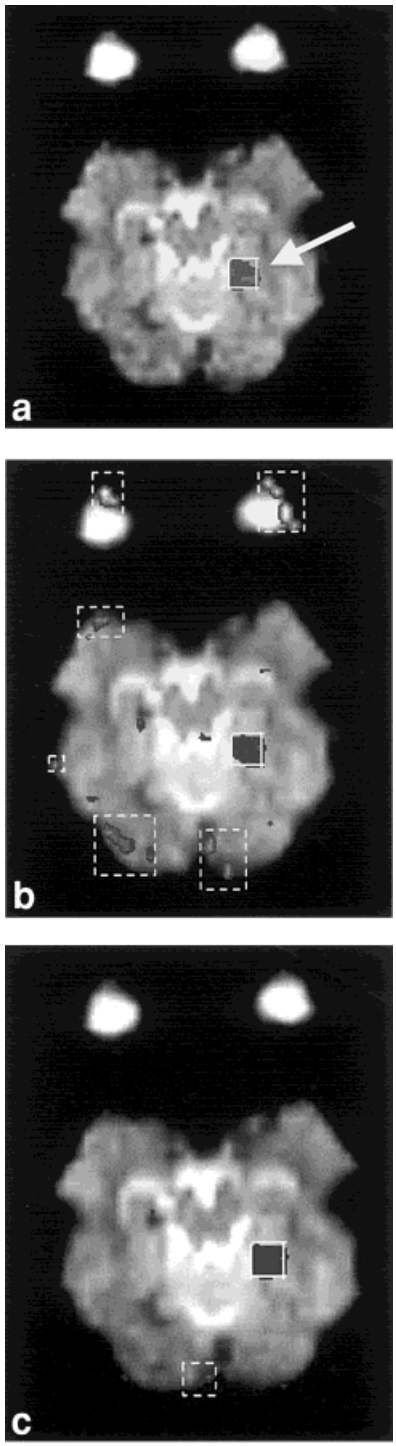

FIG. 1. **a:** An axial slice through the motion-free phantom (with noise) showing simulated activation within the ROI (arrow). **b:** Activation in the rigid-body motion phantom in the same slice. Some strongly activated pixels outside the ROI are highlighted with a dashed-line box. All of the activated pixels outside the ROI are considered false-positive activations. **c:** Activation in the same slice after rigid-body motion was corrected using SPM99b (see text). The number of false-positive activations (in dashed-line box) is reduced. All activation was determined using a *t*-test ($P < 0.05$).

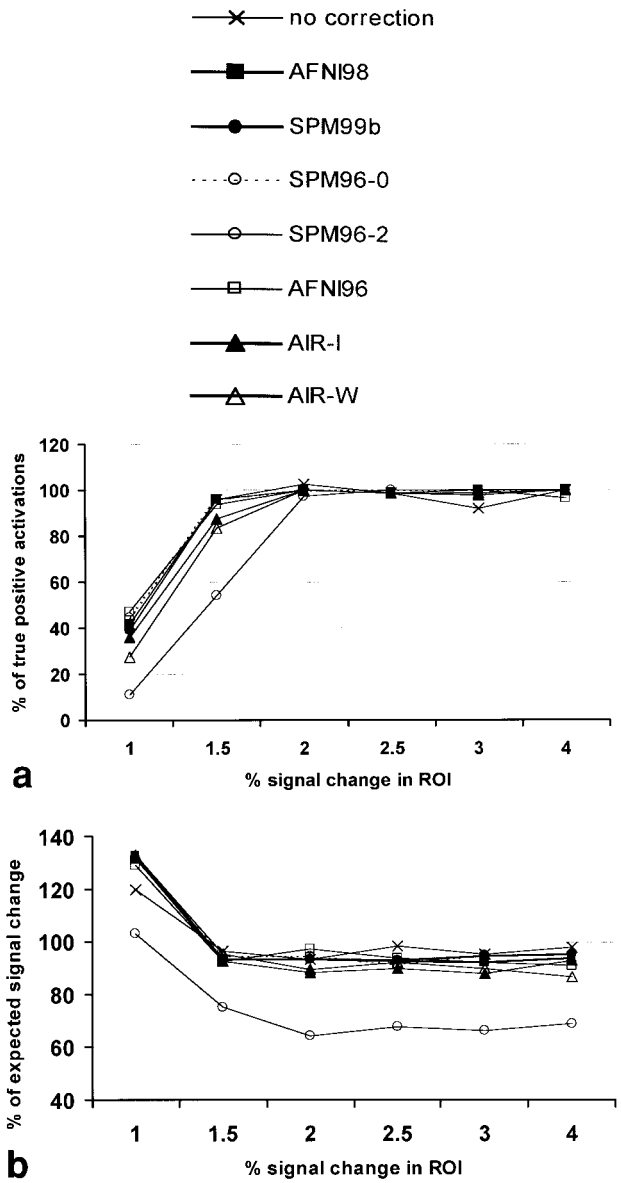

FIG. 2. **a:** Percent of true-positive activations vs. percent signal change in the ROI. **b:** Percent of expected signal change in the region vs. percent of signal change in the ROI in the rigid-body motion phantom.

activation due to noise. In Fig. 1b the same slice is shown in the rigid-body motion phantom. The activation due to motion is apparent. Some of these areas are highlighted by dashed-line boxes. The same slice after rigid-body motion is corrected by SPM99b (8) is shown in Fig. 1c.

In the activation-only phantom (motion-free), all algorithms except SPM96-2 were able to retain 100% of the activated pixels and percent signal change present prior to realignment. With SPM96-2 there was no activation detected at levels less than 4% signal change.

Figures 2a and 3a show the percent of true-positive activations in the region vs. the level of activation in the region for the rigid-body phantom and the elastic-motion phantom, respectively. The percent of expected signal change in the region vs. the level of activation in the region for each phantom is shown in Figs. 2b and 3b. In all of these figures, the ideal result is 100%. Figure 4 shows the number of false-positive activations after each type of correction, and prior to any correction for all three phantoms.

DISCUSSION

The activation-only phantom was created to determine whether image data unaffected by motion will be altered by the application of motion correction algorithms. In cases where the activation data is preserved, it is implied

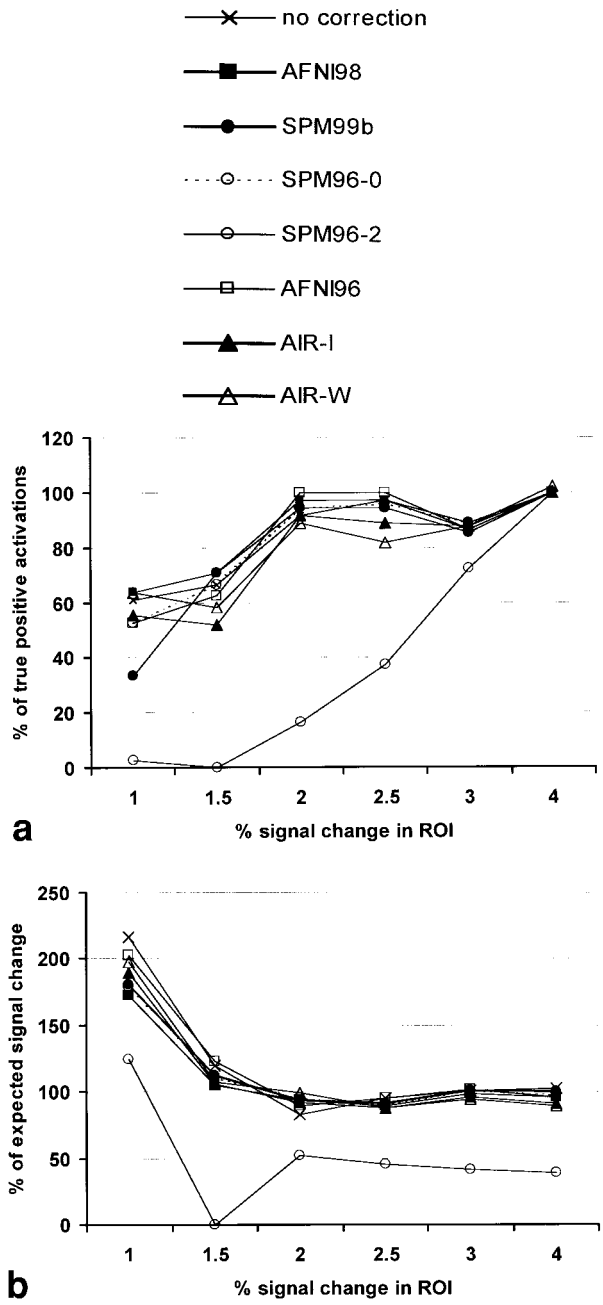

FIG. 3. **a:** Percent of true-positive activations vs. percent signal change in the ROI. **b:** Percent of expected signal change in the region vs. percent of signal change in the ROI in the elastic-motion phantom.

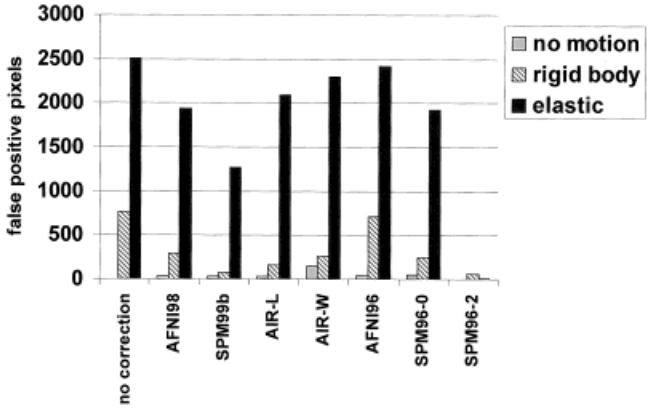

FIG. 4. Number of false-positive activations in the activation-only phantom, the rigid-body motion phantom, and the elastic-motion phantom after realignment with each algorithm and prior to any realignment.

that the algorithm may be considered for use on all data sets. Otherwise, some threshold of motion would have to be set. All of the programs studied maintained the correct activation in the absence of motion except for SPM96-2. This algorithm removed all false-positive activations in addition to many true-positive activations. Using AFNI98, SPM99b and AIR-L, the number of false-positive activations is similar to those without correction. There were slightly more false-positive activations when the 2D realignment AFNI96 and SPM96-0 was used. There was a large increase in false-positive activations using AIR-W.

The data using the rigid-body phantom is more diverse than the activation-only data. For most algorithms, the percent of true-positive activations and percent signal change are accurate for activation levels of 1.5% or higher. This is true even when no realignment is performed. At 1% signal change, the added noise decreased the true-positive activations and increased the percent signal change in the ROI. Added motion and realignment did not significantly alter this. The SPM96-2 results show a decrease in all activation levels, while greatly reducing the numbers of activated pixels at the lowest activation levels. Figure 4 shows that the number of false-positive activations is relatively high if no motion correction is performed. All programs except AFNI96 greatly reduce this error, with SPM99b and SPM96-2 having results closest to the motion-free data.

The elastic-motion phantom includes nonrigid, localized motion within the volume to represent apparent image distortion due to cerebral spinal fluid and blood pulsatility. This more complicated motion produces more error in the activation maps than does rigid-body motion. For the elastic-motion phantom, the activation is accurate at signal increases of 2% or higher after most realignments and without realignment. Only the SPM96-2 reduces signal changes and number of activated pixels at these levels. The number of false-positive activations is higher in this phantom than in the rigid-body phantom. The only realignment that can reduce these without removing true-positive activations is SPM99b.

To determine the accuracy of realignment, the standard deviation of the center of mass in the *x*, *y*, and *z* directions after each realignment was measured. No correlation was found between these measures and the activation parameters studied. In fact, SPM96-2 had the best realignment results and the worst activation results. This information, coupled with the fact that SPM96-2 removed true-positive activations even when no motion was initially present, indicates that the resampling may be the primary cause of error in some of these algorithms. In some cases the errors caused by resampling may be greater than the benefits of the accurate realignment. This underscores the importance of this study in enabling comparisons of algorithms based on activation rather than realignment. That would lead to the identification of those algorithms which can optimize results by minimizing false-positive activations through accurate realignment while maximizing true-positive activations through accurate resampling.

In summary, these data illustrate that the computer-generated phantom can be used to examine the effects of different realignment algorithms on different types of motion. The results from this study show that image sets that are not affected by motion can be corrected by many of these techniques without degradation of the activation. Similarly, the data from the phantoms before realignment imply that the primary error in these data is specificity, i.e., the number of false-positive activations is highest prior to realignment. It is clear that the realignment techniques differ in their results for the three parameters chosen. Therefore, the technique applied in a study should be based on the specific goals of the experiment. This same strategy can be used to examine other types of motion, such as task-correlated motion (4). Further, the levels of activation can be increased to more appropriately model activation levels found at 3T or higher.

REFERENCES

1. Ogawa S, Lee TM, Nayak AS, Glynn P. Oxygenation sensitive contrast in magnetic resonance imaging of rodent brain at high magnetic fields. Magn Reson Med 1990;14:68–78.
2. Malonek D, Grinvald A. Interactions between electrical activity and cortical microcirculation revealed by imaging spectroscopy: implications for functional brain mapping. Science 1996;272:551–554.
3. Kennan RP, Scanley BE, Innis RB, Gore JC. Physiological basis for BOLD MR signal changes due to neuronal stimulation: separation of blood volume and magnetic susceptibility effects. Magn Reson Med 1998;40:840–846.
4. Hajnal JV, Myers R, Oatridge A, Schwieso JE, Young IR, Bydder GM. Artifacts due to stimulus correlated motion in functional imaging of the brain. Magn Reson Med 1994;31:283–291.
5. Cox RW. AFNI: software for analysis and visualization of functional magnetic resonance neuroimages. Comput Biomed Res 1996;29:162–173.
6. Woods RP, Grafton ST, Holmes CJ, Cherry SR, Mazziotta JC. Automated image registration: I. General methods and intrasubject, intramodality validation. J Comput Assist Tomogr 1998;22:139–152.
7. Woods RP, Grafton ST, Watson JDG, Sicotte NL, Mazziotta JC. Automated image registration: II. Intersubject validation of linear and nonlinear models. J Comput Assist Tomogr 1998;22:153–165.
8. Friston KJ, Jezzard P, Turner R. The analysis of functional MRI time-series. Hum Brain Mapp 1994;1:153–171.
9. Bedell BJ, Narayana PA, Johnston DA. Three dimensional MR image registration of the human brain. Magn Reson Med 1996;35:384–390.
10. Biswal BB, Hyde JS. Contour-based registration technique to differentiate between task-activated and head motion-induced signal variations in fMRI. Magn Reson Med 1997;38:470–476.

11. Maas LC, Frederick BD, Renshaw PF. Decoupled automated rotational and translational registration for functional MRI time series data: the DART registration algorithm. Magn Reson Med 1997;37:131–139.
12. Singh M, Al-Dayeh L, Patel P, Kim T. Correction for head movements in multi-slice EPI functional MRI. IEEE Trans Nucl Sci 1998;45:2162–2167.
13. Cox RW, Jesmanowicz A. Real-time 3D image registration for functional MRI. Magn Reson Med 1999;42:1014–1018.
14. Pelizzari CA, Chen GTY, Spelbring DR, Weichselbaum RR, Chen CT. Accurate three-dimensional registration of CT, PET, and/or MR images of the brain. J Comput Assist Tomogr1989;13:20–26.
15. Strupp JP. Stimulate: a GUI based fMRI analysis software package. NeuroImage 1996;3:S607.
16. Hartmann SL, Parks MH, Schlack H, Riddle WR, Price RR, Martin PR, Dawant BM. Automatic computation of brain and cerebellum volumes in normal subjects and chronic alcoholics. In: Proceedings of IPMI, 1999;1613:430–435.